



## OPEN ACCESS

## EDITED BY

Klaus Okkenhaug,  
University of Cambridge, United Kingdom

## REVIEWED BY

Dirk Baumjohann,  
University Hospital Bonn, Germany  
Alessio Mazzoni,  
University of Florence, Italy

## \*CORRESPONDENCE

Lucy S. K. Walker  
✉ lucy.walker@ucl.ac.uk

RECEIVED 04 March 2024

ACCEPTED 15 May 2024

PUBLISHED 29 May 2024

## CITATION

Edner NM, Houghton LP, Ntavli E, Rees-Spear C, Petersone L, Wang C, Fabri A, Elfaki Y, Rueda Gonzalez A, Brown R, Kisand K, Peterson P, McCoy LE and Walker LSK (2024) TIGIT<sup>+</sup>Tfh show poor B-helper function and negatively correlate with SARS-CoV-2 antibody titre. *Front. Immunol.* 15:1395684. doi: 10.3389/fimmu.2024.1395684

## COPYRIGHT

© 2024 Edner, Houghton, Ntavli, Rees-Spear, Petersone, Wang, Fabri, Elfaki, Rueda Gonzalez, Brown, Kisand, Peterson, McCoy and Walker. This is an open-access article distributed under the terms of the [Creative Commons Attribution License \(CC BY\)](https://creativecommons.org/licenses/by/4.0/). The use, distribution or reproduction in other forums is permitted, provided the original author(s) and the copyright owner(s) are credited and that the original publication in this journal is cited, in accordance with accepted academic practice. No use, distribution or reproduction is permitted which does not comply with these terms.

# TIGIT<sup>+</sup>Tfh show poor B-helper function and negatively correlate with SARS-CoV-2 antibody titre

Natalie M. Edner<sup>1</sup>, Luke P. Houghton<sup>1</sup>, Elisavet Ntavli<sup>1</sup>, Chloe Rees-Spear<sup>1</sup>, Lina Petersone<sup>1</sup>, Chunjing Wang<sup>1</sup>, Astrid Fabri<sup>1</sup>, Yassin Elfaki<sup>1</sup>, Andrea Rueda Gonzalez<sup>1</sup>, Rachel Brown<sup>1,2</sup>, Kai Kisand<sup>3</sup>, Pärt Peterson<sup>3</sup>, Laura E. McCoy<sup>1</sup> and Lucy S. K. Walker<sup>1\*</sup>

<sup>1</sup>Division of Infection and Immunity, Institute of Immunity and Transplantation, University College London, London, United Kingdom, <sup>2</sup>Queen Square Institute of Neurology, University College London, London, United Kingdom, <sup>3</sup>Institute of Biomedicine and Translational Medicine, University of Tartu, Tartu, Estonia

Circulating follicular helper T cells (cTfh) can show phenotypic alterations in disease settings, including in the context of tissue-damaging autoimmune or anti-viral responses. Using severe COVID-19 as a paradigm of immune dysregulation, we have explored how cTfh phenotype relates to the titre and quality of antibody responses. Severe disease was associated with higher titres of neutralising S1 IgG and evidence of increased T cell activation. ICOS, CD38 and HLA-DR expressing cTfh correlated with serum S1 IgG titres and neutralising strength, and interestingly expression of TIGIT by cTfh showed a negative correlation. TIGIT<sup>+</sup>cTfh expressed increased IFN $\gamma$  and decreased IL-17 compared to their TIGIT<sup>-</sup>cTfh counterparts, and showed reduced capacity to help B cells *in vitro*. Additionally, TIGIT<sup>+</sup>cTfh expressed lower levels of CD40L than TIGIT<sup>-</sup>cTfh, providing a potential explanation for their poor B-helper function. These data identify phenotypic changes in polyclonal cTfh that correlate with specific antibody responses and reveal TIGIT as a marker of cTfh with altered function.

## KEYWORDS

follicular helper T cells, antibody response, TIGIT, B cell help, COVID-19

## 1 Introduction

Follicular helper T cells (Tfh) are important mediators of humoral immune responses, providing help to B cells for the production of high-affinity antibodies during germinal centre (GC) reactions (1). While Tfh exert their function predominantly in the B cell follicles of secondary lymphoid organs, blood-borne counterparts of Tfh cells exist, termed circulating Tfh (cTfh) (2, 3). Analysis of cTfh is an area of growing interest, with

suggestions that these cells could potentially serve as biosensors for advanced immunomonitoring or predictive modelling (4–8). In the setting of autoimmunity, where inappropriate immune responses cause tissue damage, the frequency of cTfh has been shown to be elevated and can correlate with pathogenic autoantibodies (9–11). Similarly, following infections or vaccination, cTfh expressing activation markers, such as ICOS and CD38, are transiently increased and correlate with antibody levels (12–15).

To further explore cTfh phenotype in a setting of immune dysregulation, we have used cryopreserved peripheral blood mononuclear cell (PBMC) samples from the first wave of the COVID-19 pandemic in which exposure-naïve individuals responded to the original Wuhan strain of SARS-CoV-2. While the majority of infections resulted in only mild disease symptoms, some infected individuals developed more severe disease, requiring hospital care and admission to intensive care units (ICUs), and we have focussed on the latter individuals here.

Both the innate and adaptive arm of the immune system are known to be critical for control of SARS-CoV-2 infection and a dysregulated immune response has been linked to severe disease outcomes. Infection with SARS-CoV-2 also induces neutralising antibodies and CD4 and CD8 T cells responses, which orchestrate viral control (16–19). It has been suggested that in elderly individuals these three arms of the adaptive immune response are imbalanced providing at least a partial explanation for the higher risk of developing severe COVID-19 seen in this age group (18, 20). Neutralising antibodies, which often target the receptor binding domain within the S1 subunit of the viral spike protein, have been shown to correlate with protection from reinfection and severe disease and are the target for successful vaccination strategies (21, 22). An increase in activated cTfh has also been documented following SARS-CoV-2 infection (23–26).

In an interesting twist, humoral immunity can also compromise responses to SARS-CoV-2 as illustrated by the discovery that neutralising antibodies to type I interferon (IFN) can be found in about 20% of patients with severe COVID-19 (27, 28). Here, pre-existing autoimmunity dysregulates the innate antiviral response, interfering with the precisely controlled production of type I IFN required to orchestrate immunity. Notably, a delay or impairment of the type I IFN response has been associated with increased viral loads and severe disease (29–33) and several SARS-CoV-2 proteins have been found to antagonise components of the IFN response (34, 35).

In this study, we have applied high-dimensional immunophenotyping of PBMC samples from a cohort of hospitalised COVID-19 patients, focusing in particular on the cTfh compartment and how it relates to the anti-SARS-CoV-2 specific antibody response and disease severity. We found evidence of increased activation of CD4 and CD8 T cells as well as higher S1 IgG antibody titres and stronger neutralising antibodies in severe disease. Additionally, we observed that TIGIT expression by cTfh was inversely correlated with S1 IgG antibody titres. This prompted additional investigation into the nature of TIGIT expressing cTfh. Our findings demonstrate that TIGIT<sup>+</sup> cTfh are skewed towards a Tfh1 phenotype and have a lower capacity to provide B cell help *in vitro*, potentially attributable to their inferior expression of CD40L.

## 2 Materials and methods

### 2.1 Study participant details

Samples of individuals hospitalised at Royal Free Hospital, London, United Kingdom, with COVID-19 were cryopreserved and stored in the Royal Free London Biobank (NRES 16/WA/0298). Samples were collected from April to June 2020. SARS-CoV-2 infection was confirmed by PCR-based testing and disease severity was assessed according to supplemental oxygen requirements and ICU admission in the duration of hospitalisation (see patient information in [Supplementary Table 1](#)). For three individuals no positive PCR test result could be obtained at the time of blood collection, however a diagnosis of SARS-CoV-2 infection was assigned by the treating physicians on the basis of clinical symptoms. In total, PBMCs from 36 patients (16 no suppl. oxygen, 12 suppl. oxygen, 8 ICU) and serum samples from a subset of these patients (2 no suppl. oxygen, 5 suppl. oxygen, 8 ICU) were obtained. The protocol and consent document of this study were approved by appropriate independent ethics committees or institutional review boards. Peripheral blood of self-declared healthy individuals was collected at the UCL Institute of Immunity and Transplantation, London, United Kingdom.

### 2.2 Sample preparation

Cryopreserved samples were thawed in a 37°C water bath and vial contents transferred to a 50 mL Falcon tube containing 10 ml pre-warmed C10 media (RPMI+ (RPMI 1640 (Thermo Fisher) + 2 mM L-Glutamine (Thermo Fisher) + 100 U Penicillin-Streptomycin (Thermo Fisher) + 50 µM 2-Mercaptoethanol (Sigma)) + 10% foetal calf serum (FCS, PAN-Biotech)). After centrifugation at 400 × g for 7 minutes cell pellet was resuspended in 10 ml pre-warmed C10 media.

Peripheral blood mononuclear cells (PBMCs) were isolated from whole blood by density gradient centrifugation. In brief, whole blood was diluted in phosphate-buffered saline (PBS, Thermo Fisher) and layered over Histopaque 1077 (Merck) in LeucoSep 50 ml tubes (Greiner Bio-One). After centrifugation at 800 × g for 15 minutes with no brake, supernatant above barrier was poured into new 50 ml Falcon tube and centrifuged at 350 × g for 10 minutes to remove remaining histopaque. Supernatant was discarded and pellet resuspended in PBS + 2% FCS (P2). Platelets were removed by centrifugation at 250 × g for 10 minutes. The resulting pellet was resuspended in P2.

### 2.3 Anti-IFN autoantibody assay

The sequences encoding IFN $\alpha$  subtypes (IFN $\alpha$ 1, IFN $\alpha$ 2, IFN $\alpha$ 8, IFN $\alpha$ 21) or IFN $\lambda$  subtypes IFN $\lambda$ 1–3 (IL-29, IL-28A, IL-28B) were cloned into pPK-CMV-F4 plasmid (PromoCell GmbH) where NanoLuc luciferase sequence (Promega) was inserted instead of firefly luciferase. HEK293 cells were transfected with the constructs, 72 hours later cell media containing the secreted

fusion proteins was collected. Patient sera were diluted 1:10 using buffer A (50 mM Tris pH 7.5, 100 mM NaCl, 5 mM MgCl<sub>2</sub>, 1% Triton X-100), 25  $\mu$ L serum dilution and 25  $\mu$ L of protein G agarose bead suspension (Exalpha Biologicals) was incubated in a 96-well microfilter plate (Merck Millipore) at room temperature for 1 hour. The next 1-hour incubation step was carried out after the addition of either IFN $\alpha$  subtype mix or IFN $\lambda$  subtype mix of fusion proteins corresponding to 1  $\times$  10<sup>6</sup> LUs (luminescent unit) for each. A vacuum system (Millipore) was used to wash away the unbound fusion proteins. Nano-Glo<sup>®</sup> Luciferase Assay (Promega) and VICTOR X Multilabel Plate Reader (PerkinElmer Life Sciences) was used to quantify luminescence. The same three AAB negative control serum samples were run in duplicates with each 96-well plate. For each sample a fold change of luminescence relative to the mean of three negative control samples was calculated by dividing the mean luminescence value of the test sample with the mean of the negative control samples.

## 2.4 Neutralisation assay

HIV-1 particles pseudotyped with SARS-CoV-2 spike were produced in a T75 flask seeded the day before with 3 million HEK293T/17 cells in 10ml complete DMEM, supplemented with 10% FBS, 100IU/ml penicillin and 100 $\mu$ g/ml streptomycin. Cells were transfected using 60 $\mu$ g of PEI-Max (Polysciences) with a mix of three plasmids: 9.1 $\mu$ g HIV-1 luciferase reporter vector (36), 9.1 $\mu$ g HIV-1 p8.91 packaging construct and 1.4 $\mu$ g WT SARS-CoV-2 spike expression vector (36). Supernatants containing pseudotyped virions were harvested 48 h post-transfection, filtered through a 0.45- $\mu$ m filter and stored at -80°C. Neutralisation assays were conducted by serial dilutions of sera in DMEM (10% FBS and 1% penicillin-streptomycin) and incubated with pseudotyped virus for 1 h at 37°C in 96-well plates. HeLa cells stably expressing ACE-2 (provided by J.E. Voss, Scripps Institute) were then added to the assay (10,000 cells per 100 $\mu$ l per well). After 48–72 h, luminescence was assessed as a proxy of infection by lysing cells with the Bright-Glo luciferase kit (Promega), using a Glomax plate reader (Promega). Measurements were performed in duplicate and used to calculate 50% inhibitory dilution values in GraphPad Prism software.

## 2.5 Semiquantitative ELISA

As described previously (37), nine columns of a half-well 96-well MaxiSorp plate were coated with purified SARS-CoV-2 spike S1 protein in PBS (3 $\mu$ g/ml per well in 25 $\mu$ l) and the remaining three columns were coated with 25 $\mu$ l goat anti-human F(ab)<sup>2</sup> diluted 1:1000 in PBS to generate the internal standard curve. After incubation at 4°C overnight, the ELISA plate was blocked for 1 h in assay buffer (PBS, 5% milk, 0.05% Tween 20). Sera was diluted in assay buffer at dilutions from 1:50 to 1:5000 and 25 $\mu$ l added to the ELISA plate. Serial dilutions of known concentrations of IgG standards were applied to the three standard curve columns in

place of sera. The ELISA plate was then incubated for 2 h at room temperature and then washed 4 times with PBS-T (PBS, 0.05% Tween 20). Alkaline phosphatase-conjugated goat anti-human IgG at 1:1000 dilution was then added to each well and incubated for 1 h. Following this, plates were washed 6 times with PBS-T and 25 $\mu$ l of colorimetric alkaline phosphatase substrate added. Absorbance was measured at 405nm. Antigen-specific IgG concentrations in serum were then calculated based on interpolation from the IgG standard results using a four-parameter logistic (4PL) regression curve fitting model.

## 2.6 Flow cytometry

PBMCs of COVID-19 patients and healthy controls were stained with panels of antibody cocktails as described in [Supplementary Table 2](#). Typically, 1–2  $\times$  10<sup>6</sup> cells were stained per sample. Samples were acquired on a BD LSRFortessa (BD Biosciences) or a Cytex Aurora (Cytex Biosciences).

For cytokine staining, cells were first restimulated. COVID-19 patient samples were incubated in C10 with 10 ng/ml phorbol 12-myristate 13-acetate (PMA, Sigma) and 1  $\mu$ M ionomycin (Sigma) for four hours at 37°C with 10  $\mu$ g/ml Brefeldin A (Sigma) added for the last two hours. For cytokine staining of TIGIT<sup>+</sup> and TIGIT<sup>-</sup> Tfh after overnight  $\alpha$ CD3 stimulation, sorted cells were stimulated overnight at 37°C in C10 in 1  $\mu$ g/ml  $\alpha$ CD3 (clone: OKT3, BioXCell) coated wells with 5  $\mu$ g/ml  $\alpha$ CD28 (clone: CD28.2, Thermo Fisher). 10 ng/ml PMA and 1  $\mu$ M ionomycin were added for the last four hours and 10  $\mu$ g/ml Brefeldin A and 2  $\mu$ M Monensin (Biolegend) for the last two hours. For cytokine staining after coculture assays (as described below), either two or six days after start of the assay 10 ng/ml PMA and 1  $\mu$ M ionomycin were added for the last four hours and 10  $\mu$ g/ml Brefeldin A and 2  $\mu$ M Monensin for the last two hours.

For surface CD40L staining, PBMCs were incubated overnight at 37°C in C10 in the presence of 0.5  $\mu$ g/ml Staphylococcal Enterotoxin B (SEB). Additionally, 5  $\mu$ g/ml  $\alpha$ CD40 (clone: HB14, Biolegend) or a mouse IgG1 $\kappa$  isotype (clone: P3.6.2.8.1, Thermo Fisher) was added. For intracellular CD40L staining, PBMCs were incubated overnight at 37°C in C10 in the presence of 0.5  $\mu$ g/ml SEB. For the last two hours of the incubation 10  $\mu$ g/ml Brefeldin A were added.

## 2.7 Coculture assays

Coculture assays of B cells and Tfh cells were performed as previously described (38). Briefly, B cells and T cells were sorted using a BD FACSAria Fusion (BD Biosciences) (see [Supplementary Table 2](#) for sorting panels) and cocultured at a 1:1 ratio for six days at 37°C in C10 in the presence of 100 ng/ml SEB. For TIGIT blocking experiments, 1  $\mu$ g/ml  $\alpha$ TIGIT (clone: A15153G, Biolegend) or a mouse IgG2 $\kappa$  isotype (clone: MOPC-173, Biolegend) was added at the start of the culture. Assays were performed in duplicate.

## 2.8 Data analysis

Flow cytometry data were analysed using FlowJo v.10 (BD Biosciences). For unsupervised clustering, pregated live, singlet lymphocytes were preprocessed in R v.4.0.2 as previously described (5) and the FlowSOM algorithm as implemented in the Bioconductor package CATALYST v.1.14.1 was used to identify CD4 and CD8 T cell populations. FlowSOM clustering was then applied again on these T cell populations and optimal number of clusters was identified using delta area plots. UMAP plots of flow cytometry data were generated from downsampled data using the CATALYST package. Heatmaps were generated using the CATALYST package. Publicly available single cell multi-omics data from the COMBAT study (39) was analysed using the CRAN packages Seurat v.5 (40) and scGate v.1.6 (41). Plots were produced using the CRAN packages ggplot2 v.3.4.4, ggpvr v.0.6.0, ggforestplot v.0.1.0, ggthemes v.5.0.0, gtable v.0.4.3, scales v.1.3.0, colorspace v.2.1-0, cowplot v.1.1.3, scico v.1.5.0, and circlize v.0.4.15. Data cleaning and formatting was carried out using CRAN packages dplyr v.1.1.4, tidyr v.1.3.1, reshape2 v.1.4.4, and Rmisc v.1.5.1. Statistical calculations were performed in R v.4.0.2. Statistical test used and N numbers (number of individuals) are indicated in figure legends. A p value of less than 0.05 was considered significant.

## 3 Results

### 3.1 Severe COVID-19 is associated with distinct T cell phenotypes

Cryopreserved PBMCs isolated from the blood of 36 individuals hospitalised with COVID-19 between March and June 2020 were used for deep immunophenotyping using two spectral flow cytometry panels, with matched serum samples analysed for antibody levels. Disease severity was assessed based on supplemental oxygen requirements, with patients exhibiting most severe disease requiring ICU admission. Analysis of anti-IFN autoantibodies revealed two patients with high titres of anti-IFN $\alpha$  autoantibodies, one of which also exhibited anti-IFN $\lambda$  autoantibodies (Figure 1A). Both of these individuals were admitted to ICU consistent with a more severe disease course observed in patients harbouring anti-IFN autoantibodies (27, 28).

Immune cell lineage subsets were identified using FlowSOM clustering (Figure 1B, Supplementary Figures 1A, B) and no major changes were observed other than a drop in NK cell frequency in patients that received supplemental oxygen (Figure 1C, Supplementary Figures 1C, D). To better understand the impact of severe COVID-19 on the T cell compartment we performed FlowSOM clustering on CD4 and CD8 T cells from both spectral flow cytometry panels (Supplementary Figure 2). Twelve FlowSOM clusters were found to be significantly different in patients that required supplemental oxygen or ICU admission compared to patients with no supplemental oxygen requirements (Figures 2A–C). Clusters with elevated frequencies in severe COVID-19 showed high expression of the proliferation marker

Ki67 (Panel 2: CD4 clusters G & I and CD8 clusters J & L) as well as activation markers, such as CD38, HLA-DR and ICOS in both CD4 and CD8 T cells (Panel 1: CD4 cluster A and CD8 clusters D, E & F; Panel 2: CD4 clusters G, H & I and CD8 clusters J & L). In some of

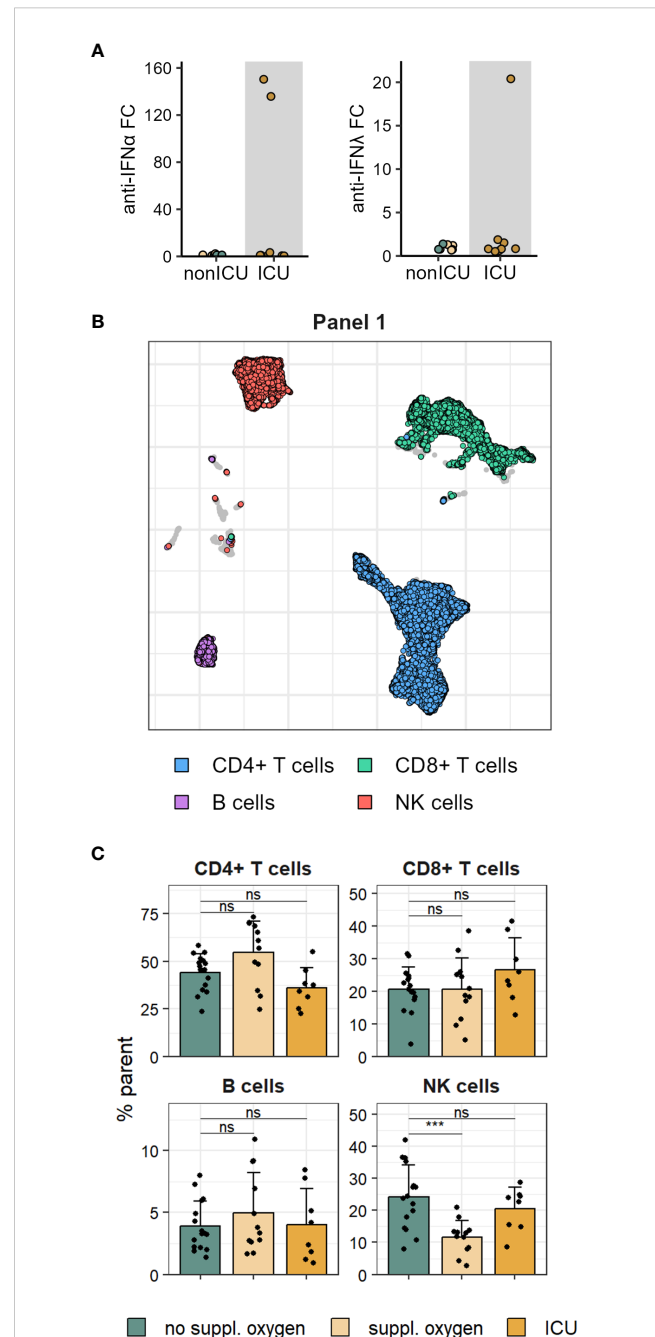


FIGURE 1

Proportions of major immune cell lineage are mostly unchanged in mild and severe COVID-19. (A) Serum anti-IFN $\alpha$  (left) and anti-IFN $\lambda$  (right) autoantibodies measured in patients admitted to ICU and non-ICU patients. (B) UMAP of immune cell subsets in PBMCs stained with flow cytometry Panel 1. (C) Frequencies of Panel 1 immune cell subsets shown in B in disease severity groups. Shown are means + SD. No suppl. oxygen, n = 16; Suppl. oxygen, n = 12; ICU, n = 8. Kruskal-Wallis (CD4<sup>+</sup> T cells, p = 0.022; CD8<sup>+</sup> T cells, p = 0.370; B cells, p = 0.685; NK cells, p = 0.001) followed by two-tailed Mann-Whitney U-test; \*\*\*p < 0.001; ns, not significant.

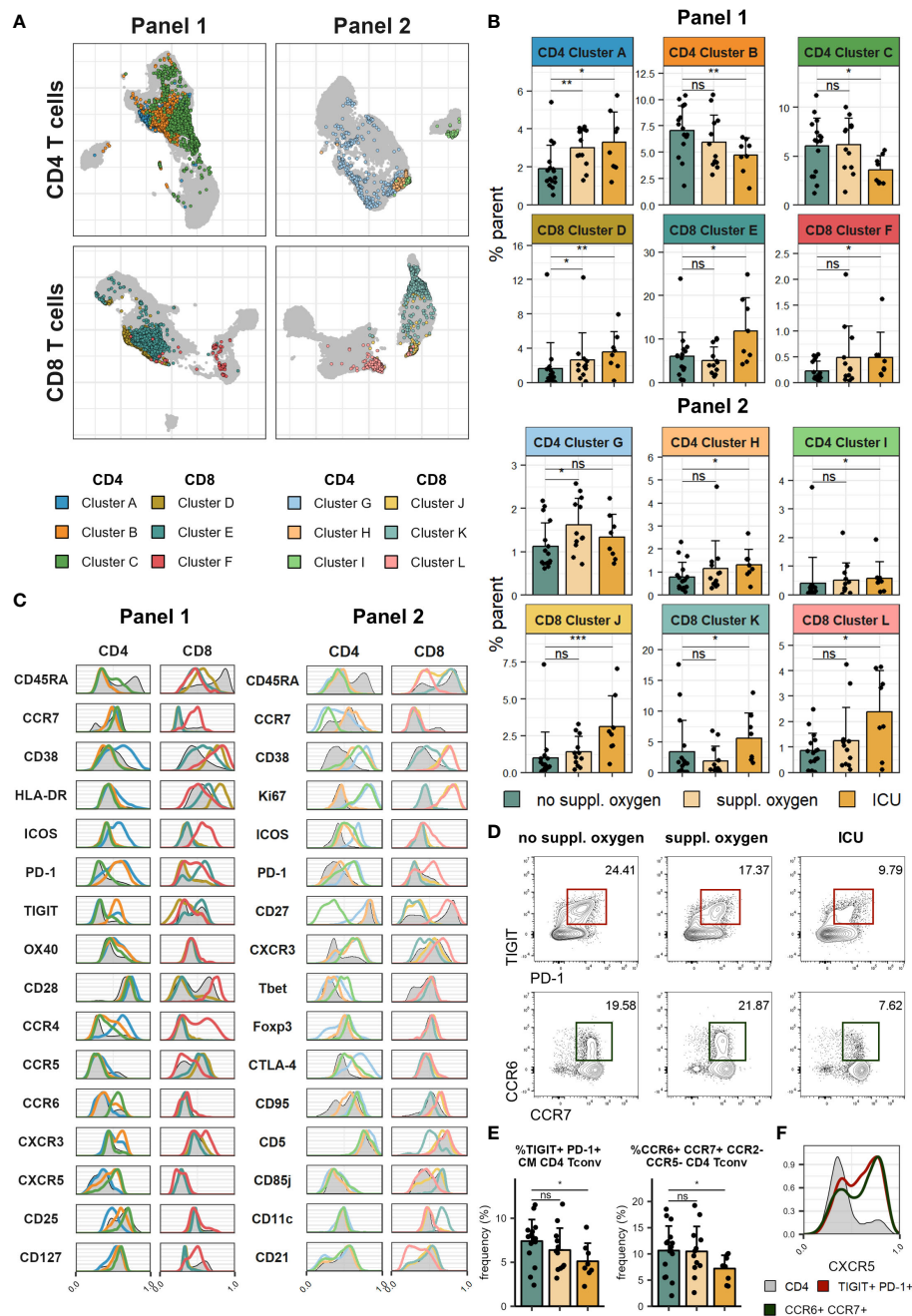


FIGURE 2

Severe COVID-19 is associated with increased T cell activation and proliferation. Cryopreserved PBMCs of individuals hospitalised with COVID-19 were analysed using two spectral flow cytometry panels. (A) UMAP of CD4 (top) and CD8 (bottom) T cells in Panel 1 (left) and Panel 2 (right). Highlighted clusters are significantly different in frequency in disease severity groups. (B) Frequencies of clusters within CD4 and CD8 T cells of Panel 1 (top) and Panel 2 (bottom) significantly different between disease severity groups. (C) Histograms of marker expression of CD4 and CD8 T cell clusters (colour) and all CD4 and CD8 T cells (grey) in Panel 1 (left) and Panel 2 (right). (D) Representative flow cytometry plots of TIGIT<sup>+</sup>PD-1<sup>+</sup> CM CD4 Tconv (top) and CCR6<sup>+</sup>CCR7<sup>+</sup>CCR2<sup>-</sup>CCR5<sup>-</sup> CD4 Tconv (bottom). (E) Frequency of TIGIT<sup>+</sup>PD-1<sup>+</sup> CM CD4 Tconv (left) and CCR6<sup>+</sup>CCR7<sup>+</sup>CCR2<sup>-</sup>CCR5<sup>-</sup> CD4 Tconv (right) in disease severity groups. (F) Representative histograms of CXCR5 expression of TIGIT<sup>+</sup>PD-1<sup>+</sup> CM CD4 Tconv (red), CCR6<sup>+</sup>CCR7<sup>+</sup>CCR2<sup>-</sup>CCR5<sup>-</sup> CD4 Tconv (green) and all CD4 T cells (grey). In (B, E) means + SD are shown. No suppl. oxygen, n = 16; Suppl. oxygen, n = 12; ICU, n = 8. Kruskal-Wallis (Cluster A, p = 0.008; Cluster B, p = 0.051; Cluster C, p = 0.060; Cluster D, p = 0.010; Cluster E, p = 0.050; Cluster F, p = 0.131; Cluster G, p = 0.069; Cluster H, p = 0.110; Cluster I, p = 0.080; Cluster J, p = 0.003; Cluster K, p = 0.034; Cluster L, p = 0.116; TIGIT<sup>+</sup>PD-1<sup>+</sup> CM CD4 Tconv, p = 0.080; CCR6<sup>+</sup>CCR7<sup>+</sup>CCR2<sup>-</sup>CCR5<sup>-</sup> CD4 Tconv, p = 0.084) followed by two-tailed Mann-Whitney U-test; \*\*\*p < 0.001; \*\*p < 0.01; \*p < 0.05; ns, not significant.

these clusters we also detected high levels of Tbet and CXCR3 (Panel 2: CD4 cluster I and CD8 clusters J & L), indicative of a type 1 immune response, and lack of CD28 and CD27 expression (Panel 1: CD8 clusters D & E; Panel 2: CD4 cluster I and CD8 clusters J & K), suggestive of a terminally differentiated T cell phenotype. We also identified two clusters of CD4 T cells that were significantly decreased in patients that required ICU admission (Panel 1: CD4 clusters B & C). Further examination of the phenotype of these clusters allowed us to devise manual gating strategies that reflected the frequencies found by FlowSOM clustering (Figures 2D, E, Supplementary Figures 3A, B). One of these clusters (Panel 1 CD4 cluster B) comprised central memory T cells with high expression of the coinhibitory receptors PD-1 and TIGIT, while the other (Panel 1 CD4 cluster C) was marked by distinctive expression of chemokine receptors, including high

expression of CCR6 and CCR7 and lack of CCR2 and CCR5 expression. Of potential interest, both of these clusters were enriched for CXCR5 expression, suggesting that they comprise subsets of cTfh (Figure 2F).

We examined cytokine expression of T cells following restimulation and found lower frequencies of both CD4 and CD8 T cells that co-expressed IFN $\gamma$  and TNF $\alpha$  in ICU patients (Figures 3A, B). Conversely, the CD8 T cells of these patients exhibited significantly higher levels of granzyme B (Figures 3A, C). Granzyme B expression of CD8 T cells correlated positively with frequency of one CD8 T cell cluster identified by FlowSOM (Panel 1 CD8 cluster E, Supplementary Figure 3C) which lacked CD28 expression and showed high expression of PD-1 and TIGIT. This cluster could conceivably represent the source of granzyme B expressing CD8 T cells in our dataset.

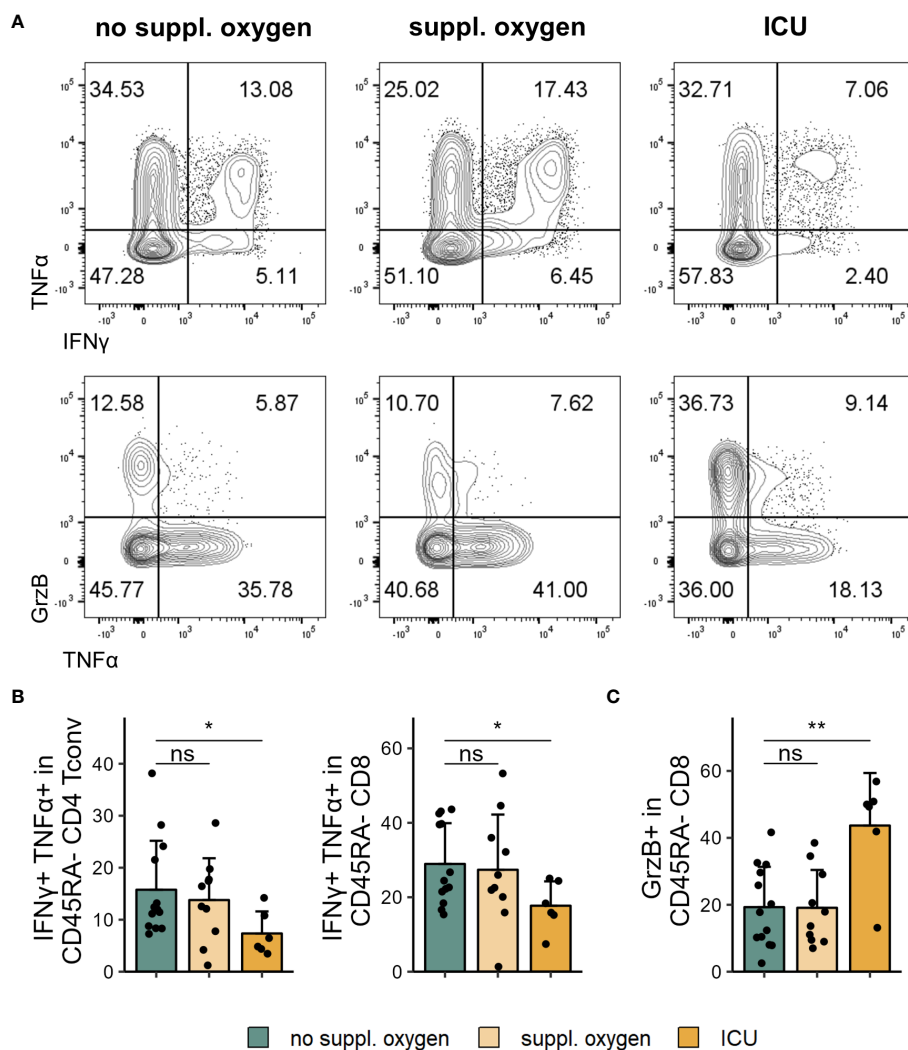


FIGURE 3

Cytokine profile changes in severe COVID-19. Cryopreserved PBMCs of individuals hospitalised with COVID-19 were restimulated and analysed for cytokine expression using flow cytometry. (A) Representative flow cytometry plots of IFN $\gamma$ <sup>+</sup>TNF $\alpha$ <sup>+</sup> (top) and GrzB<sup>+</sup> and TNF $\alpha$ <sup>+</sup> (bottom) in CD45RA<sup>-</sup> CD8 T cells. (B) Frequencies of IFN $\gamma$ <sup>+</sup>TNF $\alpha$ <sup>+</sup>CD45RA<sup>-</sup> CD4 Tconv (left) and CD8 (right) in disease severity groups. (C) Frequencies of GrzB<sup>+</sup>CD45RA<sup>-</sup> CD8 in disease severity groups. Shown are means + SD. No suppl. oxygen, n = 16; Suppl. oxygen, n = 12; ICU, n = 8. Kruskal-Wallis test (IFN $\gamma$ <sup>+</sup>TNF $\alpha$ <sup>+</sup>CD45RA<sup>-</sup> CD4 Tconv, p = 0.086; IFN $\gamma$ <sup>+</sup>TNF $\alpha$ <sup>+</sup>CD45RA<sup>-</sup> CD8, p = 0.120; GrzB<sup>+</sup>CD45RA<sup>-</sup> CD8, p = 0.011) followed by two-tailed Mann-Whitney U-test; \*\*p < 0.01; \*p < 0.05; ns, not significant.

### 3.2 Higher expression of TIGIT on cTfh is inversely correlated with S1 IgG titres

The generation of robust antibody responses, particularly against the receptor binding domain of the S1 subunit of the spike protein, is important for protection from severe COVID-19 disease upon reinfection (21, 42). Titres of S1 IgG (high: > 200 µg/ml, medium: 25–200 µg/ml, low: < 25 µg/ml) as well as the strength of neutralising antibodies (measured as reciprocal ID50; potent: > 4050, strong: 1350–4050, intermediate: 450–1350, weak: 100–450, no neutralisation: < 100) were previously assessed for this patient cohort (43). When stratifying these by disease severity we found that more severe disease was associated with higher S1 IgG titres as well as stronger neutralising antibodies (Figures 4A, B;  $p=0.0098$  and  $p=0.0133$  for S1 IgG titre and nAb respectively, Fisher's exact test).

Frequencies of cTfh are increased following infection and vaccination (12–14, 26) and SARS-CoV-2 specific Tfh have been shown to correlate with neutralising antibody responses in convalescent individuals (44). We were interested to understand how cTfh frequency and phenotype related to the titres and neutralising strength of SARS-CoV-2 specific antibodies in our patient cohort.

There were no statistically significant changes in the frequencies of cTfh (CD45RA<sup>-</sup>CXCR5<sup>+</sup>, for gating strategy see Supplementary Figure 4A) with increased antibody titres and neutralising strengths (Figure 4C). However, we found significantly increased frequencies of ICOS and CD38 expressing cTfh from individuals with high S1 IgG titres and stronger neutralising antibodies (Figure 4D). Similarly, higher expression of HLA-DR was linked to S1 IgG titre and neutralising strength (Figure 4D). While there was a trend for PD-1 expression to be elevated in individuals with detectable S1 IgG this was not statistically significant (Figure 4D). Another receptor highly expressed by Tfh is the coinhibitory receptor TIGIT (45), however its role in Tfh function is not well defined. Interestingly, when we probed expression of TIGIT on cTfh we saw that it was significantly lower in individuals with high S1 IgG titres and there was a trend for reduced TIGIT frequencies in individuals with strong neutralising antibodies (Figure 4E). This observation was even more striking when comparing TIGIT<sup>+</sup> cTfh to ICOS<sup>+</sup>CD38<sup>+</sup> cTfh; the ratio was lower in the high S1 IgG titre and potent neutralising antibody groups (Figure 4F). Consistent with the association between severe disease and higher S1 IgG titre and neutralising capacity, we also found that the ratio of TIGIT<sup>+</sup> cTfh to ICOS<sup>+</sup>CD38<sup>+</sup> cTfh was lower in severe disease (Figure 4G).

Since TIGIT<sup>+</sup> cTfh were negatively correlated with S1 IgG antibodies, we wondered whether TIGIT expressing and non-expressing cTfh exhibited phenotypic differences that could explain this observation. We therefore examined expression of molecules linked to Tfh function on both TIGIT<sup>+</sup> and TIGIT<sup>-</sup> cTfh cells. Against our expectations, we found that TIGIT<sup>+</sup> cTfh showed slightly higher expression of ICOS and CD38 compared to TIGIT<sup>-</sup> cTfh while there was no difference in HLA-DR and OX40 levels (Figure 5A). TIGIT<sup>+</sup> cTfh expressed higher levels of PD-1 than TIGIT<sup>-</sup> cTfh (Figure 5A), however, this cannot by itself explain the negative relationship between cTfh TIGIT expression and S1

IgG titres since PD-1 expression on cTfh was not different between individuals with low and high S1 IgG titres, as shown in Figure 4D. We went on to examine the chemokine receptor expression of TIGIT<sup>+</sup> and TIGIT<sup>-</sup> cTfh and found that TIGIT<sup>+</sup> cTfh showed higher levels of CXCR5 and CXCR3, while TIGIT<sup>-</sup> cTfh were higher in expression of CCR7, CCR6, CCR2 and CCR5 (Figure 5B). Tfh subsets are classically defined by their expression of the chemokine receptors CXCR3 and CCR6 (46) (Figure 5C). We found that TIGIT expressing cTfh were skewed towards a CXCR3<sup>+</sup>CCR6<sup>-</sup>Tfh1 phenotype while CXCR3<sup>-</sup>CCR6<sup>+</sup>Tfh17 cells were more prominent in TIGIT<sup>-</sup> cTfh (Figure 5D).

TIGIT expression has been reported on regulatory T cells, including follicular regulatory T cells, which are able to negatively regulate GC responses (45, 47, 48). While we found a significantly higher frequency of CD25<sup>hi</sup>CD127<sup>lo</sup> cells within TIGIT<sup>+</sup> compared to TIGIT<sup>-</sup> cTfh (Supplementary Figures 4B, C), excluding these cells from our cTfh gating did not alter the negative association of TIGIT<sup>+</sup> cTfh with S1 IgG titres (Supplementary Figure 4D). Follicular regulatory T cell frequencies and TIGIT expression by follicular regulatory T cells did not differ between groups.

### 3.3 TIGIT expression demarks Tfh with reduced capacity for B cell help and lower production of IL-17 and CD40L

Having established that TIGIT expression on cTfh is lower in individuals with high S1 IgG titres we wondered whether TIGIT<sup>+</sup> cTfh were perhaps less capable of supporting B cell help than their TIGIT<sup>-</sup> counterparts. To address this question, we isolated TIGIT<sup>+</sup> and TIGIT<sup>-</sup> cTfh as well as naïve B cells from healthy individuals and cocultured them for six days in the presence of staphylococcal enterotoxin B (SEB) (Figure 6A). Naïve B cells cultured with TIGIT<sup>-</sup> cTfh showed greater CD38 upregulation than naïve B cells cultured with TIGIT<sup>+</sup> cTfh consistent with an increased capacity of TIGIT<sup>-</sup> cTfh to provide B cell help in this *in vitro* setting (Figure 6B). To test whether TIGIT signalling directly impaired B cell helper function of cTfh, we cocultured cTfh and naïve B cells in the presence of a TIGIT blocking antibody. The capacity of cTfh to provide help to B cells was not significantly altered by TIGIT blockade, suggesting that TIGIT expression may instead mark a population of Tfh with reduced helper capacity (Supplementary Figure 5A).

To test for phenotypic differences between TIGIT<sup>+</sup> and TIGIT<sup>-</sup> cTfh, we assessed expression of a panel of cytokines either after overnight activation with  $\alpha$ CD3 or after coculture with naïve B cells for two or six days. It has previously been reported that TIGIT<sup>+</sup> cTfh produce high levels of IL-21 (49, 50), which can support plasma cell differentiation *in vitro* (51, 52). While we found a trend of higher IL-21 expression of TIGIT<sup>+</sup> cTfh after overnight activation, after coculture with naïve B cells for six days TIGIT<sup>-</sup> cTfh were producing significantly more IL-21 than TIGIT<sup>+</sup> cTfh (Supplementary Figure 5B). At some of the time points examined, TIGIT<sup>-</sup> cTfh also produced more IL-2, an important factor for T cell survival and proliferation, as well as IL-10, which can also support B cell differentiation (53) (Supplementary Figure 5B). We observed no differences in IL-4 expression, another cytokine produced by Tfh

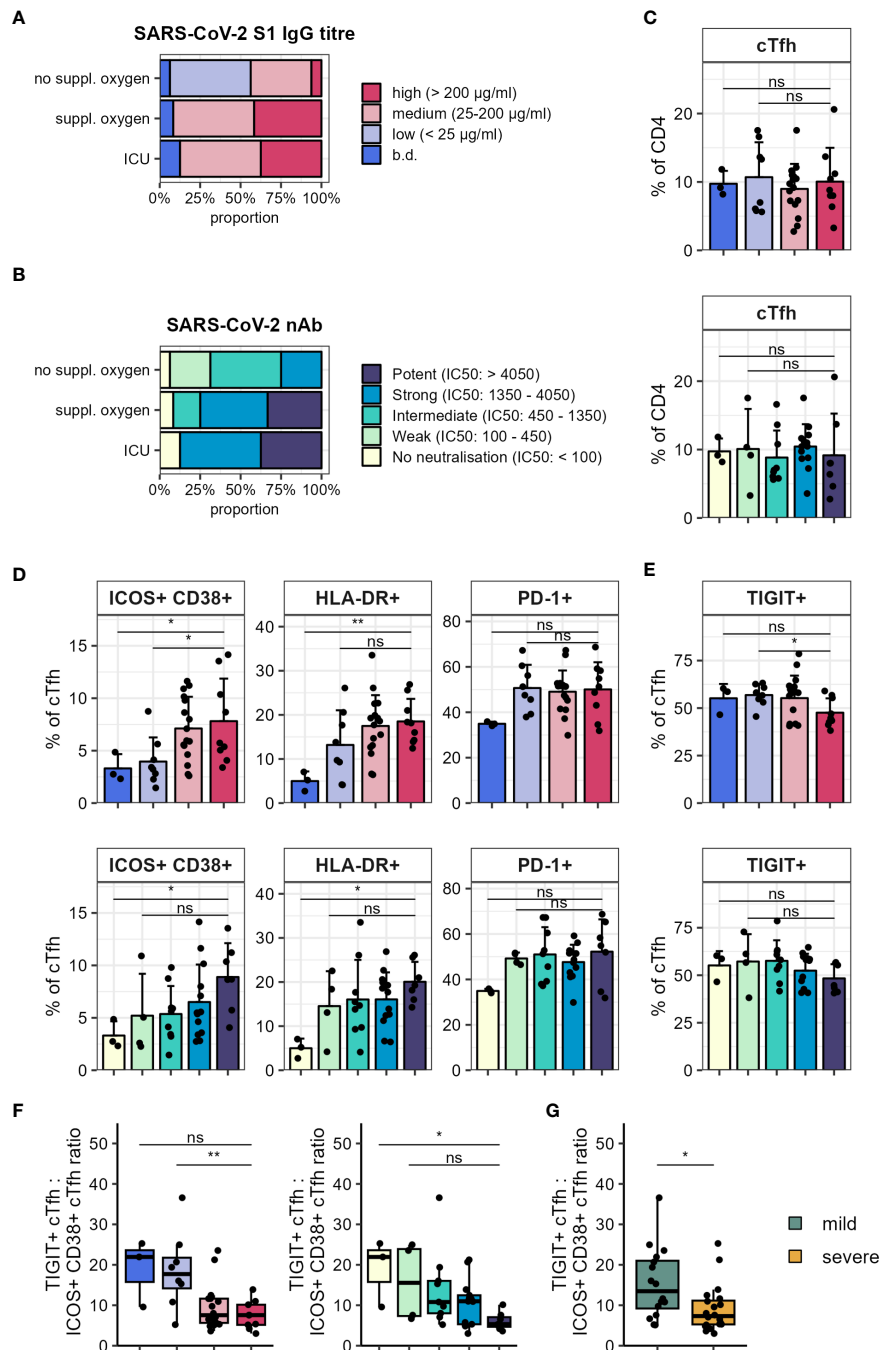


FIGURE 4

Circulating Tfh subsets correlate with serum anti-SARS-CoV-2 antibodies. Serum S1 IgG titres and neutralising reciprocal ID50 were measured in patients hospitalised with COVID-19. (A) Anti-SARS-CoV-2 S1 IgG titre in disease severity groups. (B) Anti-SARS-CoV-2 neutralising antibody strength in disease severity groups. (C) Frequency of cTfh (CD45RA<sup>-</sup>CXCR5<sup>+</sup>) in S1 IgG titre (top) and nAb strength (bottom) groups. (D) Frequency of indicated marker expression in cTfh in S1 IgG titre (top) and nAb strength (bottom) groups. (E) Frequency of TIGIT expression in cTfh in S1 IgG titre (top) and nAb strength (bottom) groups. (F) Ratio of TIGIT<sup>+</sup> cTfh to ICOS<sup>+</sup>CD38<sup>+</sup> cTfh in S1 IgG titre (left) and nAb strength (right) groups. (G) Ratio of TIGIT<sup>+</sup> cTfh to ICOS<sup>+</sup>CD38<sup>+</sup> cTfh in disease severity groups (mild: no suppl. oxygen; severe: suppl. oxygen + ICU). In (A, B) proportions per group are shown. In (C–E) means + SD are shown. In (F, G) box plots are shown, with black horizontal line denoting median value, while box represents the IQRs (IQR, Q1–Q3 percentile) and whiskers show the minimum (Q1 – 1.5x IQR) and maximum (Q3 + 1.5x IQR) values. High, n = 9; medium, n = 16; low, n = 8; below detection (b.d.), n = 3. Potent, n = 7; strong, n = 13; intermediate, n = 9; weak, n = 4; no neutralisation, n = 3; mild, n = 16; severe, n = 20. Kruskal-Wallis test (S1 IgG cTfh, p = 0.947; nAb cTfh, p = 0.576; S1 IgG ICOS<sup>+</sup>CD38<sup>+</sup> cTfh, p = 0.018; S1 IgG HLA-DR<sup>+</sup> cTfh, p = 0.031; S1 IgG PD-1<sup>+</sup> cTfh, p = 0.127; nAb ICOS<sup>+</sup>CD38<sup>+</sup> cTfh, p = 0.090; nAb HLA-DR<sup>+</sup> cTfh, p = 0.066; nAb PD-1<sup>+</sup> cTfh, p = 0.156; S1 IgG TIGIT<sup>+</sup> cTfh, p = 0.189; nAb TIGIT<sup>+</sup> cTfh, p = 0.318; S1 IgG TIGIT<sup>+</sup> cTfh to ICOS<sup>+</sup>CD38<sup>+</sup> cTfh, p = 0.015; nAb TIGIT<sup>+</sup> cTfh to ICOS<sup>+</sup>CD38<sup>+</sup> cTfh, p = 0.051) followed by two-tailed Mann-Whitney U-test; \*\*p < 0.01; \*p < 0.05; ns, not significant.

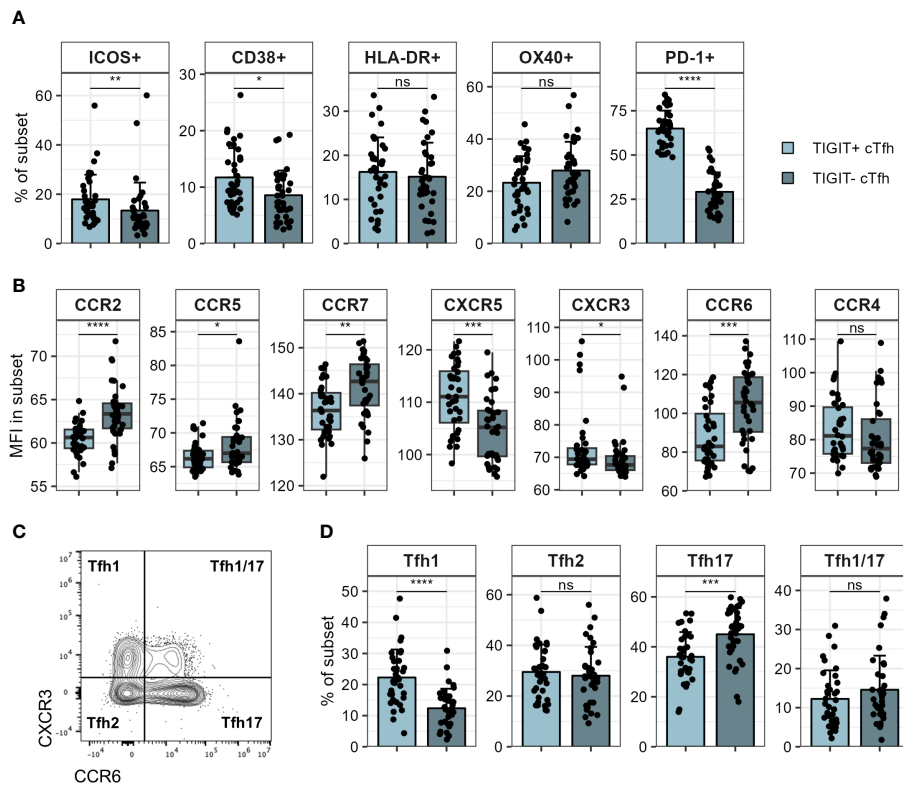


FIGURE 5

Phenotyping of TIGIT<sup>+</sup> and TIGIT<sup>-</sup> cTfh. TIGIT<sup>+</sup> and TIGIT<sup>-</sup> cTfh in PBMCs of patients hospitalised with COVID-19 were analysed for expression of various markers using flow cytometry. (A) Expression of indicated markers in TIGIT<sup>+</sup> and TIGIT<sup>-</sup> cTfh. (B) Expression of indicated chemokine receptors in TIGIT<sup>+</sup> and TIGIT<sup>-</sup> cTfh. (C) Representative flow cytometry plot of CXCR3 and CCR6 in cTfh. Tfh subsets corresponding to chemokine receptor expression pattern are indicated in each quadrant. (D) Frequency of indicated Tfh subsets in TIGIT<sup>+</sup> and TIGIT<sup>-</sup> cTfh. In (A, D) means + SD are shown. In (B) box plots are shown, with black horizontal line denoting median value, while box represents the IQRs (IQR, Q1–Q3 percentile) and whiskers show the minimum (Q1 – 1.5× IQR) and maximum (Q3 + 1.5× IQR) values. N = 36. Two-sided Wilcoxon signed-rank test; \*\*\*\*p < 0.0001; \*\*\*p < 0.001; \*\*p < 0.01; \*p < 0.05; ns, not significant.

(54) (Supplementary Figure 5B). Since analysis of chemokine receptor expression had suggested skewing of TIGIT<sup>+</sup> and TIGIT<sup>-</sup> cTfh to a Tfh1 and Tfh17 phenotype respectively, we furthermore assessed expression of IFN $\gamma$  and IL-17. TIGIT<sup>-</sup> cTfh produced significantly more IL-17 at all time points analysed while TIGIT<sup>+</sup> cTfh produced almost no IL-17 (Figures 6C, D). In contrast, TIGIT<sup>+</sup> cTfh produced higher levels of IFN $\gamma$  following overnight stimulation and after two days of coculture with B cells (Figures 6C, D). Production of IL-17 and IFN $\gamma$  is therefore consistent with Tfh subset skewing of TIGIT<sup>+</sup> and TIGIT<sup>-</sup> cTfh which we observed in COVID-19 patients (Figure 5D) as well as healthy controls (Supplementary Figure 5C).

To further understand phenotypic differences between TIGIT<sup>+</sup> and TIGIT<sup>-</sup> cTfh, we made use of the publicly available multi-omics dataset of peripheral blood immune cells from COVID-19 patients collected by the COMBAT consortium (39). Tfh that egress from lymphoid tissues and enter the blood downregulate most Tfh associated markers; while CXCR5 expression appears least affected (55), nonetheless, CXCR5 mRNA expression is sparsely detected in peripheral blood CD4 T cells (Supplementary Figure 6A) and it can be difficult to identify cTfh based on transcriptomics alone. Instead, we made use of CITE-seq protein expression data available within the COMBAT dataset and the

single cell signature scoring algorithms implemented in scGate (41) to identify CXCR5<sup>+</sup>CD45RA<sup>-</sup> Tfh-like cells in this dataset (Supplementary Figures 6B–D). Using the same approach to identify TIGIT<sup>+</sup> and TIGIT<sup>-</sup> cells within the Tfh-like cells (Supplementary Figures 6E–G) we then went on to identify genes differentially expressed between these two subsets (Supplementary Figure 6H). As expected TIGIT was expressed at higher levels within the TIGIT<sup>+</sup> cells and we could also confirm CXCR3 and CCR6 skewing on the mRNA level. Furthermore, TIGIT<sup>+</sup> cells expressed higher levels of Tfh associated markers ICOS, PDCD1 and TOX. Conversely, TIGIT<sup>-</sup> cells showed higher expression of the proliferation marker MYC and also interestingly the costimulatory molecule CD40LG. Following *in vitro* stimulation with SEB we could confirm that both surface as well as intracellular levels of CD40L were significantly higher in TIGIT<sup>-</sup> cTfh compared to TIGIT<sup>+</sup> cTfh (Figure 7). Given the importance of CD40L/CD40 interactions in driving B cell activation and differentiation in T cell dependent antibody responses, increased expression of CD40L could conceivably contribute to the superior B-helper function in TIGIT<sup>-</sup> cTfh cells.

Thus, TIGIT demarks cTfh that have reduced capability for activating B cells *in vitro* and produce lower levels of IL-17 and CD40L compared to their TIGIT<sup>-</sup> counterparts.

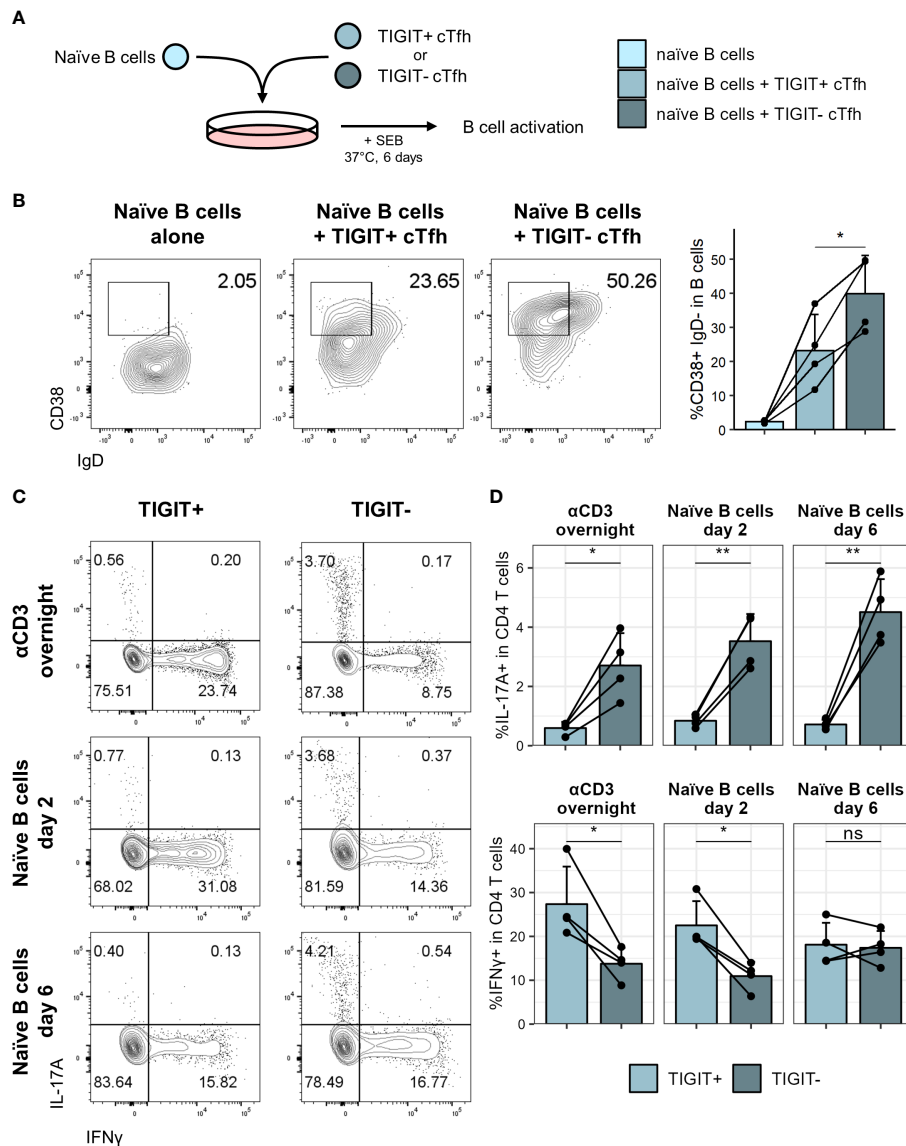


FIGURE 6

TIGIT<sup>+</sup> cTfh are poor B cell helpers *in vitro*. TIGIT<sup>+</sup> and TIGIT<sup>-</sup> cTfh (CXCR5<sup>+</sup>CD45RA<sup>+</sup>CD4<sup>+</sup>CD3<sup>+</sup>) from PBMCs of self-declared healthy individuals were cocultured with autologous naïve B cells (IgD<sup>+</sup>CD27<sup>-</sup>CD19<sup>+</sup>) to assess B cell helper function. (A) T:B coculture setup. (B) Representative flow cytometry plots (left) and collated data (right) of CD38<sup>+</sup>IgD<sup>-</sup> B cells following coculture of naïve B cells with TIGIT<sup>+</sup> or TIGIT<sup>-</sup> cTfh. (C) Representative flow cytometry plots of IL-17 and IFN $\gamma$  expression in TIGIT<sup>+</sup> (left) and TIGIT<sup>-</sup> (right) cTfh after overnight stimulation (top) or coculture with naïve B cells for two (middle) or six (bottom) days. (D) Frequency of IL-17 (top) and IFN $\gamma$  (bottom) expression in TIGIT<sup>+</sup> and TIGIT<sup>-</sup> Tfh following overnight stimulation (left) or coculture with naïve B cells for two (middle) or six (right) days. Shown are means + SD. Data is representative of four independent experiments. N = 4. Two-sided paired Student's t test; \*\*p < 0.01; \*p < 0.05; ns, not significant.

## 4 Discussion

The quality of the antibody response is profoundly shaped by the nature of the T cells providing B cell help. Here, we have identified a relationship between subsets of peripheral blood Tfh and the anti-S1 serum antibody response in a cohort of patients hospitalised with COVID-19. While the main role of Tfh is within the GC, counterparts of these GC Tfh can be found in the circulation (6) and links between cTfh subsets, particularly ICOS and CD38 expressing cTfh, and antigen specific antibody responses have previously been reported following vaccination

(12, 56, 57). We corroborate these findings here in the setting of SARS-CoV-2 infection, showing higher frequencies of cTfh expressing ICOS, CD38 as well as HLA-DR within the peripheral blood of individuals with higher S1 IgG titres and stronger neutralising antibodies. Furthermore, we find a previously unreported, negative association between the anti-S1 antibody response and cTfh expressing the coinhibitory receptor TIGIT, with higher frequencies of TIGIT expressing cTfh found in individuals with lower S1 IgG titres. Tfh are known to express high levels of TIGIT, particularly within the GC. Its role in Tfh function, however, is incompletely understood although it has

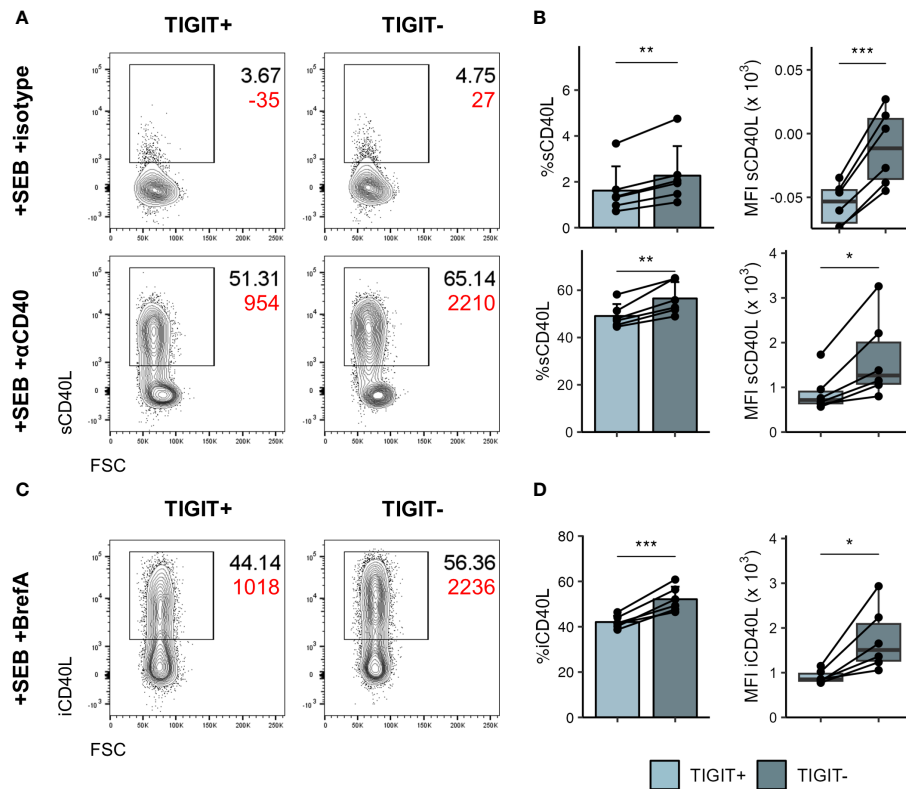


FIGURE 7

TIGIT<sup>-</sup> cTfh produce more CD40L following stimulation. PBMCs of self-declared healthy individuals were stimulated overnight with SEB to assess CD40L production. (A) Representative flow cytometry plots of surface CD40L expression in TIGIT<sup>+</sup> (left) and TIGIT<sup>-</sup> (right) cTfh after overnight stimulation in presence of isotype (top) or anti-CD40 (bottom) antibody. Black text represents frequency, red text represents MFI. (B) Collated frequency (left) and MFI (right) of surface CD40L expression in TIGIT<sup>+</sup> and TIGIT<sup>-</sup> cTfh in presence of isotype (top) or anti-CD40 (bottom). (C) Representative flow cytometry plots of intracellular CD40L expression in TIGIT<sup>+</sup> (left) and TIGIT<sup>-</sup> (right) cTfh after overnight stimulation in presence of Brefeldin A. Black text represents frequency, red text represents MFI. (D) Frequency (left) and MFI (right) of intracellular CD40L expression in TIGIT<sup>+</sup> and TIGIT<sup>-</sup> cTfh. In (B, D) on the left means + SD are shown. In (B, D) on the right box plots are shown, with black horizontal line denoting median value, while box represents the IQRs (IQR, Q1–Q3 percentile) and whiskers show the minimum (Q1 – 1.5× IQR) and maximum (Q3 + 1.5× IQR) values. Data is representative of two independent experiments. N = 6. Two-sided paired Student's t test; \*\*\*p < 0.001; \*\*p < 0.01; \*p < 0.05.

been suggested that within the GC it may insulate Tfh from signals received through CD226, a costimulatory receptor that shares its ligands with TIGIT (58).

We further demonstrate that TIGIT<sup>-</sup> cTfh are superior to TIGIT<sup>+</sup> cTfh in their ability to activate B cells in *in vitro* coculture assays. This does not appear to be mediated by TIGIT itself as TIGIT blocking antibodies had no effect on Tfh mediated B cell activation. Indeed, Yasutomi et al. showed that CD112 and CD155, the shared ligands of TIGIT and CD226, are not expressed by tonsillar B cells. Instead, these ligands are predominantly expressed by CD14<sup>+</sup> monocytes and CD11c<sup>+</sup> conventional dendritic cells (58), making these antigen presenting cells the more likely interaction partner for both CD226 and TIGIT expressed on T cells. TIGIT therefore appears to instead demark a population of cTfh cells that are less capable of providing help during B cell activation. We show that following *in vitro* activation TIGIT<sup>+</sup> cTfh express lower levels of CD40L, a critical mediator of T-dependent (TD) antibody responses known to promote B cell activation, proliferation and differentiation (59). While both TIGIT<sup>+</sup> and TIGIT<sup>-</sup> cTfh were able to upregulate CD40L following activation, TIGIT<sup>-</sup> cTfh did so to a higher extent.

This difference in CD40L expression could therefore, at least partially, explain the difference in B cell activation observed in coculture assays.

Aside from CD40L, we also found that TIGIT<sup>+</sup> and TIGIT<sup>-</sup> cTfh displayed a distinct cytokine profile. Cytokines produced by Tfh play a key role in shaping TD antibody responses and of these the importance of IL-21 and IL-4 in shaping the GC reaction is well recognised (60, 61). Previous reports suggested that TIGIT expressing cTfh produce high levels of IL-21 following *in vitro* stimulation (49, 50). While we did see a trend for higher amounts of IL-21 following overnight activation, in the longer coculture assays we found TIGIT<sup>-</sup> cTfh produced more IL-21 than TIGIT<sup>+</sup> cTfh, with no difference in IL-4 production. Furthermore, we identified that IFN $\gamma$  and IL-17 were differentially expressed in TIGIT<sup>+</sup> and TIGIT<sup>-</sup> cTfh. Both cytokines can be produced by Tfh and have been shown to influence GC reactions, with IL-17 reported to promote TD antibody responses (62–64) while the role of IFN $\gamma$  appears to be more ambiguous (65–69). These cytokines are also typically linked to Th1 and Th17 subsets and, in line with this, we found IFN $\gamma$  producing TIGIT<sup>+</sup> cTfh to be predominantly CXCR3<sup>+</sup>CCR6<sup>-</sup> Tfh1, while IL-17 producing TIGIT<sup>-</sup> cTfh were skewed towards a CXCR3<sup>-</sup>

CCR6<sup>+</sup> Tfh17 phenotype. Interestingly, a recent study by He et al. found that CXCR3<sup>-</sup> cTfh (isolated from healthy, COVID-19 convalescent individuals or vaccine recipients) were superior in their capacity to activate B cells in coculture compared with their CXCR3<sup>+</sup> cTfh counterparts (70), mirroring our observations in the TIGIT<sup>+</sup> versus TIGIT<sup>-</sup> cTfh compartments. Thus, a preference for cytokine usage in particular Tfh subsets may be another contributing factor to the superior ability of TIGIT<sup>-</sup> cTfh to promote B cell activation *in vitro*.

The demonstration that severe COVID-19 is associated with higher titres of neutralising S1 IgG as well as increased frequencies of CD4 and CD8 T cells expressing CD38, HLA-DR and Ki67 is consistent with reports from other patient cohorts where increased immune activation was linked to severe disease (25, 36, 43, 71). It is difficult to disentangle whether these observations are linked to an overactive, and perhaps inappropriate, immune response or are rather due to higher viral loads that may have been present in individuals experiencing more severe disease, perhaps facilitated by a diminished NK cell population (72). Nonetheless, these findings suggest the possibility of using peripheral immune cell subsets as biomarkers for disease severity.

A major outstanding question remains regarding how peripheral blood TIGIT<sup>-</sup> cTfh subsets relate to Tfh in secondary lymphoid organs. While clonal relationships between circulating and GC Tfh have been established (3, 73), it is thought that cTfh predominantly arise from pre-Tfh at the T-B border and not the GC itself, demonstrated by the presence of cTfh in SAP deficient individuals with impaired T-B interactions (2). Results published by Yasutomi et al. provide insight into transcriptional differences of TIGIT<sup>+</sup> and TIGIT<sup>-</sup> Tfh isolated from human tonsils (58). They conclude that TIGIT<sup>+</sup> Tfh are more differentiated and less proliferative than TIGIT<sup>-</sup> Tfh and have a GC Tfh phenotype. During an ongoing immune response an influx of activated ICOS<sup>+</sup>CD38<sup>+</sup> but TIGIT<sup>-</sup> pre-Tfh could conceivably shift the balance of TIGIT<sup>-</sup> and TIGIT<sup>+</sup> cTfh within the circulation, leading to a proportional decrease in TIGIT<sup>+</sup> cTfh. Future work investigating the clonal relationship between TIGIT<sup>+</sup> and TIGIT<sup>-</sup> Tfh in secondary lymphoid organs and the blood would provide further insight here, and inclusion of TIGIT analysis will enhance efforts to exploit cTfh as a biomarker population in the context of vaccination, infection and autoimmunity.

## Data availability statement

The raw data supporting the conclusions of this article will be made available by the authors, without undue reservation.

## Ethics statement

The studies involving humans were approved by UCL–Royal Free Hospital BioBank Ethical Review Committee Reference number: NC2020.24 NRES EC number: 16/WA/0289. The studies

were conducted in accordance with the local legislation and institutional requirements. The participants provided their written informed consent to participate in this study.

## Author contributions

NE: Formal Analysis, Investigation, Methodology, Visualization, Writing – original draft, Writing – review & editing. LH: Investigation, Writing – review & editing. EN: Investigation, Methodology, Writing – review & editing. CR-S: Investigation, Writing – review & editing. LP: Investigation, Writing – review & editing. CW: Investigation, Writing – review & editing. AF: Investigation, Writing – review & editing. YE: Investigation, Writing – review & editing. AR: Investigation, Writing – review & editing. RB: Data curation, Writing – review & editing. KK: Investigation, Writing – review & editing. PP: Investigation, Writing – review & editing. LM: Funding acquisition, Supervision, Writing – review & editing. LW: Conceptualization, Funding acquisition, Methodology, Project administration, Supervision, Writing – original draft, Writing – review & editing.

## Funding

The author(s) declare financial support was received for the research, authorship, and/or publication of this article. This work was supported by UCLH BRC award BRC732/JJK/101400 and a Wellcome Investigator award (220772/Z/20/Z) to LW. LM was supported by a Medical Research Council career development award (MR/R008698/1). KK and PP were supported by an Estonian Research Council grant (PRG1117). This study was also funded by the UCL Coronavirus Response Fund, made possible through generous donations from UCL's supporters, alumni, and friends (awards made to LM and LW).

## Acknowledgments

We gratefully acknowledge the support of the Tissue Access for Patient Benefit Initiative at the Royal Free Hospital. The authors would like to thank members of the ICL Centre for Clinical Microbiology for processing patient material, James E Voss of the Scripps Research Institute for the gift of HeLa ACE2-expressing cells used in neutralisation assays and Peter Cherepanov of the Francis Crick Institute for recombinant S1 antigen.

## Conflict of interest

The authors declare that the research was conducted in the absence of any commercial or financial relationships that could be construed as a potential conflict of interest.

The author(s) declared that they were an editorial board member of Frontiers, at the time of submission. This had no impact on the peer review process and the final decision.

## Publisher's note

All claims expressed in this article are solely those of the authors and do not necessarily represent those of their affiliated organizations, or those of the publisher, the editors and the

reviewers. Any product that may be evaluated in this article, or claim that may be made by its manufacturer, is not guaranteed or endorsed by the publisher.

## Supplementary material

The Supplementary Material for this article can be found online at: <https://www.frontiersin.org/articles/10.3389/fimmu.2024.1395684/full#supplementary-material>

## References

- Crotty S. T follicular helper cell biology: A decade of discovery and diseases. *Immunity*. (2019) 50:1132–48. doi: 10.1016/j.immuni.2019.04.011
- He J, Tsai LM, Leong YA, Hu X, Ma CS, Chevalier N, et al. Circulating precursor CCR7(lo)PD-1(hi) CXCR5<sup>+</sup> CD4<sup>+</sup> T cells indicate Tfh cell activity and promote antibody responses upon antigen reexposure. *Immunity*. (2013) 39:770–81. doi: 10.1016/j.immuni.2013.09.007
- Heit A, Schmitz F, Gerdt S, Flach B, Moore MS, Perkins JA, et al. Vaccination establishes clonal relatives of germinal center T cells in the blood of humans. *J Exp Med*. (2017) 214:2139–52. doi: 10.1084/jem.20161794
- Herati RS, Silva LV, Vella LA, Muselman A, Alanio C, Bengsch B, et al. Vaccine-induced ICOS+CD38+ circulating Tfh are sensitive biosensors of age-related changes in inflammatory pathways. *Cell Rep Med*. (2021) 2:100262. doi: 10.1016/j.xcrm.2021.100262
- Edner NM, Heuts F, Thomas N, Wang CJ, Petersone L, Kenefeck R, et al. Follicular helper T cell profiles predict response to costimulation blockade in type 1 diabetes. *Nat Immunol*. (2020) 21:1244–55. doi: 10.1038/s41590-020-0744-z
- Walker LSK. The link between circulating follicular helper T cells and autoimmunity. *Nat Rev Immunol*. (2022) 22:567–75. doi: 10.1038/s41577-022-00693-5
- Shigehara K, Kamekura R, Ikegami I, Sakamoto H, Yanagi M, Kamiya S, et al. Circulating T follicular helper 2 cells, T follicular regulatory cells and regulatory B cells are effective biomarkers for predicting the response to house dust mite sublingual immunotherapy in patients with allergic respiratory diseases. *Front Immunol*. (2023) 14:1284205. doi: 10.3389/fimmu.2023.1284205
- Désy O, Bédard S, Thivierge MP, Marcoux M, Desgagnés JS, Boucharde-Boivin F, et al. T follicular helper cells expansion in transplant recipients correlates with graft infiltration and adverse outcomes. *Front Immunol*. (2024) 15:1275933. doi: 10.3389/fimmu.2024.1275933
- Kenefeck R, Wang CJ, Kapadi T, Wardzinski L, Attridge K, Clough LE, et al. Follicular helper T cell signature in type 1 diabetes. *J Clin Invest*. (2015) 125:292–303. doi: 10.1172/JCI76238
- Simpson N, Gatenby PA, Wilson A, Malik S, Fulcher DA, Tangye SG, et al. Expansion of circulating T cells resembling follicular helper T cells is a fixed phenotype that identifies a subset of severe systemic lupus erythematosus. *Arthritis Rheum*. (2010) 62:234–44. doi: 10.1002/art.25032
- Ma J, Zhu C, Ma B, Tian J, Baidoo SE, Mao C, et al. Increased frequency of circulating follicular helper T cells in patients with rheumatoid arthritis. *Clin Dev Immunol*. (2012). doi: 10.1155/2012/827480
- Bentebibel SE, Lopez S, Obermoser G, Schmitt N, Mueller C, Harrod C, et al. Induction of ICOS+CXCR3+CXCR5+ T H cells correlates with antibody responses to influenza vaccination. *Sci Transl Med*. (2013) 5:176ra32. doi: 10.1126/scitranslmed.3005191
- Locci M, Havenar-Daughton C, Landais E, Wu J, Kroenke MA, Arlehamn CL, et al. Human circulating PD-1+CXCR3-CXCR5+ memory Tfh cells are highly functional and correlate with broadly neutralizing HIV antibody responses. *Immunity*. (2013) 39:758–69. doi: 10.1016/j.immuni.2013.08.031
- Herati RS, Muselman A, Vella L, Bengsch B, Parkhouse K, Alcazar DD, et al. Successive annual influenza vaccination induces a recurrent oligoclonotypic memory response in circulating T follicular helper cells. *Sci Immunol*. (2017) 2:17. doi: 10.1126/sciimmunol.aag2152
- Zhang J, Liu W, Wen B, Xie T, Tang P, Hu Y, et al. Circulating CXCR3+ Tfh cells positively correlate with neutralizing antibody responses in HCV-infected patients. *Sci Rep*. (2019) 9:10090. doi: 10.1038/s41598-019-46533-w
- Grifoni A, Weiskopf D, Ramirez SI, Mateus J, Dan JM, Rydzynski Moderbacher C, et al. Targets of T cell responses to SARS-CoV-2 coronavirus in humans with COVID-19 disease and unexposed individuals. *Cell*. (2020) 181:1489–1501.e15. doi: 10.1016/j.cell.2020.05.015
- Sekine T, Perez-Potti A, Rivera-Ballesteros O, Strålin K, Gorin JB, Olsson A, et al. Robust T cell immunity in convalescent individuals with asymptomatic or mild COVID-19. *Cell*. (2020) 183:158–168.e14. doi: 10.1016/j.cell.2020.08.017
- Rydzynski Moderbacher C, Ramirez SI, Dan JM, Grifoni A, Hastie KM, Weiskopf D, et al. Antigen-specific adaptive immunity to SARS-CoV-2 in acute COVID-19 and associations with age and disease severity. *Cell*. (2020) 183:996–1012.e19. doi: 10.1016/j.cell.2020.09.038
- Tan AT, Linster M, Tan CW, Le Bert N, Chia WN, Kunasegaran K, et al. Early induction of functional SARS-CoV-2-specific T cells associates with rapid viral clearance and mild disease in COVID-19 patients. *Cell Rep*. (2021) 34:108728. doi: 10.1016/j.celrep.2021.108728
- Oja AE, Saris A, Ghandour CA, Kragten NAM, Hogema BM, Nossent EJ, et al. Divergent SARS-CoV-2-specific T- and B-cell responses in severe but not mild COVID-19 patients. *Eur J Immunol*. (2020) 50:1998–2012. doi: 10.1002/eji.202048908
- Khouri DS, Cromer D, Reynaldi A, Schlub TE, Wheatley AK, Juno JA, et al. Neutralizing antibody levels are highly predictive of immune protection from symptomatic SARS-CoV-2 infection. *Nat Med*. (2021) 27:1205–11. doi: 10.1038/s41591-021-01377-8
- Wei J, Pouwels KB, Stoesser N, Matthews PC, Diamond I, Studley R, et al. Antibody responses and correlates of protection in the general population after two doses of the ChAdOx1 or BNT162b2 vaccines. *Nat Med*. (2022) 28:1072–82. doi: 10.1038/s41591-022-01721-6
- Thevarajan I, Nguyen THO, Koutsakos M, Druce J, Caly L, van de Sandt CE, et al. Breadth of concomitant immune responses prior to patient recovery: a case report of non-severe COVID-19. *Nat Med*. (2020) 26:453–5. doi: 10.1038/s41591-020-0819-2
- Schultheiß C, Paschold L, Simnica D, Mohme M, Willscher E, von Wenserski L, et al. Next-generation sequencing of T and B cell receptor repertoires from COVID-19 patients showed signatures associated with severity of disease. *Immunity*. (2020) 53:442–455.e4. doi: 10.1016/j.immuni.2020.06.024
- Mathew D, Giles JR, Baxter AE, Oldridge DA, Greenplate AR, Wu JE, et al. Deep immune profiling of COVID-19 patients reveals distinct immunotypes with therapeutic implications. *Science*. (2020) 369:eabc8511. doi: 10.1126/science.369.6508.1203-1
- Koutsakos M, Rowntree LC, Hensen L, Chua BY, van de Sandt CE, Habel JR, et al. Integrated immune dynamics define correlates of COVID-19 severity and antibody responses. *Cell Rep Med*. (2021) 2:100208. doi: 10.1016/j.xcrm.2021.100208
- Bastard P, Rosen LB, Zhang Q, Michailidis E, Hoffmann HH, Zhang Y, et al. Autoantibodies against type I IFNs in patients with life-threatening COVID-19. *Science*. (2020) 370:eabd4585. doi: 10.1126/science.abd4585
- Bastard P, Gervais A, Voyer TL, Rosain J, Philippot Q, Manry J, et al. Autoantibodies neutralizing type I IFNs are present in ~4% of uninfected individuals over 70 years old and account for ~20% of COVID-19 deaths. *Sci Immunol*. (2021) 6:4340–59. doi: 10.1126/sciimmunol.abl4340
- Blanco-Melo D, Nilsson-Payant BE, Liu WC, Uhl S, Hoagland D, Moller R, et al. Imbalanced host response to SARS-CoV-2 drives development of COVID-19. *Cell*. (2020) 181:1036–1045.e9. doi: 10.1016/j.cell.2020.04.026
- Hadjadj J, Yatim N, Barnabei L, Corneau A, Bousrier J, Smith N, et al. Impaired type I interferon activity and inflammatory responses in severe COVID-19 patients. *Science*. (2020) 369:718–24. doi: 10.1126/science.abc6027
- Arunachalam PS, Wimmers F, Mok CKP, Perera RAPM, Scott M, Hagan T, et al. Systems biological assessment of immunity to mild versus severe COVID-19 infection in humans. *Science*. (2020) 369:1210–20. doi: 10.1126/science.abc6261
- Galani IE, Rovina N, Lampropoulou V, Triantafyllia V, Manioudaki M, Pavlos E, et al. Untuned antiviral immunity in COVID-19 revealed by temporal type I/III interferon patterns and flu comparison. *Nat Immunol*. (2021) 22:32–40. doi: 10.1038/s41590-020-00840-x

33. Bodansky A, Vazquez SE, Chou J, Novak T, Al-Musa A, Young C, et al. NFKB2 haploinsufficiency identified via screening for IFN- $\alpha$ 2 autoantibodies in children and adolescents hospitalized with SARS-CoV-2-related complications. *J Allergy Clin Immunol*. (2023) 151:926–930.e2. doi: 10.1016/j.jaci.2022.11.020
34. Lei X, Dong X, Ma R, Wang W, Xiao X, Tian Z, et al. Activation and evasion of type I interferon responses by SARS-CoV-2. *Nat Commun*. (2020) 11:1–12. doi: 10.1038/s41467-020-17665-9
35. Xia H, Cao Z, Xie X, Zhang X, Chen JYC, Wang H, et al. Evasion of type I interferon by SARS-CoV-2. *Cell Rep*. (2020) 33:108234. doi: 10.1016/j.celrep.2020.108234
36. Seow J, Graham C, Merrick B, Acors S, Pickering S, Steel KJA, et al. Longitudinal observation and decline of neutralizing antibody responses in the three months following SARS-CoV-2 infection in humans. *Nat Microbiol*. (2020) 5:1598–607. doi: 10.1038/s41564-020-00813-8
37. O'Nions J, Muir L, Zheng L, Rees-Spear C, Rosa A, Roustan C, et al. SARS-CoV-2 antibody responses in patients with acute leukaemia. *Leukemia*. (2021) 35:289–92. doi: 10.1038/s41375-020-01103-2
38. Gao X, Lin L, Yu D. Ex vivo culture assay to measure human follicular helper T (Tfh) cell-mediated human B cell proliferation and differentiation. *Methods Mol Biol*. (2018) 1707:111–9. doi: 10.1007/978-1-4939-7474-0\_8
39. Ahern DJ, Ai Z, Ainsworth M, Allan C, Allcock A, Angus B, et al. A blood atlas of COVID-19 defines hallmarks of disease severity and specificity. *Cell*. (2022) 185:916–938.e58. doi: 10.1016/j.cell.2022.01.012
40. Hao Y, Stuart T, Kowalski MH, Choudhary S, Hoffman P, Hartman A, et al. Dictionary learning for integrative, multimodal and scalable single-cell analysis. *Nat Biotechnol*. (2024) 42:293–304. doi: 10.1038/s41587-023-01767-y
41. Andreatta M, Berenstein AJ, Carmona SJ. scGate: Marker-based purification of cell types from heterogeneous single-cell RNA-seq datasets. *Bioinformatics*. (2022) 38:2642–4. doi: 10.1093/bioinformatics/btac141
42. Shi R, Shan C, Duan X, Chen Z, Liu P, Song J, et al. A human neutralizing antibody targets the receptor-binding site of SARS-CoV-2. *Nature*. (2020) 584:120–4. doi: 10.1038/s41586-020-2381-y
43. Rees-Spear C, Muir L, Griffith SA, Heaney J, Aldon Y, Snitselaar JL, et al. The effect of spike mutations on SARS-CoV-2 neutralization. *Cell Rep*. (2021) 34:108890. doi: 10.1016/j.celrep.2021.108890
44. Zhang J, Wu Q, Liu Z, Wang Q, Wu J, Hu Y, et al. Spike-specific circulating T follicular helper cell and cross-neutralizing antibody responses in COVID-19-convalescent individuals. *Nat Microbiol*. (2021) 6:51–8. doi: 10.1038/s41564-020-00824-5
45. Kunicki MA, Amaya Hernandez LC, Davis KL, Bacchetta R, Roncarolo M-G. Identity and diversity of human peripheral Th and T regulatory cells defined by single-cell mass cytometry. *J Immunol*. (2018) 200:336–46. doi: 10.4049/jimmunol.1701025
46. Morita R, Smitt N, Bentebibel SE, Ranganathan R, Bourdery L, Zurawski L, et al. Human blood CXCR5+CD4+ T cells are counterparts of T follicular cells and contain specific subsets that differentially support antibody secretion. *Immunity*. (2011) 34:108–21. doi: 10.1016/j.immuni.2010.12.012
47. Fuhrman CA, Yeh WI, Seay HR, Saikumar Lakshmi P, Chopra G, Zhang L, et al. Divergent phenotypes of human regulatory T cells expressing the receptors TIGIT and CD226. *J Immunol*. (2015) 195:145–55. doi: 10.4049/jimmunol.1402381
48. Wu H, Chen Y, Liu H, Xu LL, Teuscher P, Wang S, et al. Follicular regulatory T cells repress cytokine production by follicular helper T cells and optimize IgG responses in mice. *Eur J Immunol*. (2016) 46:1152–61. doi: 10.1002/eji.201546094
49. Godefroy E, Zhong H, Pham P, Friedman D, Yazdanbakhsh K. TIGIT-positive circulating follicular helper T cells display robust B-cell help functions: Potential role in sickle cell alloimmunization. *Haematologica*. (2015) 100:1415–25. doi: 10.3324/haematol.2015.132738
50. Akiyama M, Suzuki K, Yoshimoto K, Yasuoka H, Kaneko Y, Takeuchi T. Peripheral TIGIT+ T follicular helper cells that produce high levels of interleukin-21 via OX40 represent disease activity in IgG4-related disease. *Front Immunol*. (2021) 12:651357. doi: 10.3389/fimmu.2021.651357
51. Ettinger R, Sims GP, Fairhurst AM, Robbins R, da Silva YS, Spolski R, et al. IL-21 induces differentiation of human naive and memory B cells into antibody-secreting plasma cells. *J Immunol*. (2005) 175:7867–79. doi: 10.4049/jimmunol.175.12.7867
52. Bryant VL, Ma CS, Avery DT, Li Y, Good KL, Corcoran LM, et al. Cytokine-mediated regulation of human B cell differentiation into ig-secreting cells: predominant role of IL-21 produced by CXCR5+ T follicular helper cells. *J Immunol*. (2007) 179:8180–90. doi: 10.4049/jimmunol.179.12.8180
53. Rousset F, Garcia E, Defrance T, Peronne C, Vezzio N, Hsu DH, et al. Interleukin 10 is a potent growth and differentiation factor for activated human B lymphocytes. *Proc Natl Acad Sci U.S.A.* (1992) 89:1890–3. doi: 10.1073/pnas.89.5.1890
54. King IL, Mohrs M. IL-4-producing CD4+ T cells in reactive lymph nodes during helminth infection are T follicular helper cells. *J Exp Med*. (2009) 206:1001–7. doi: 10.1084/jem.20090313
55. Baumjohann D, Preite S, Reboldi A, Ronchi F, Ansel KM, Lanzavecchia A, et al. Persistent antigen and germinal center B cells sustain T follicular helper cell responses and phenotype. *Immunity*. (2013) 38:596–605. doi: 10.1016/j.immuni.2012.11.020
56. Bentebibel SE, Khurana S, Schmitt N, Kurup P, Mueller C, Obermoser G, et al. ICOS + PD-1 + CXCR3 + T follicular helper cells contribute to the generation of high-avidity antibodies following influenza vaccination. *Sci Rep*. (2016) 6:26494. doi: 10.1038/srep26494
57. Huber JE, Ahlfeld J, Scheck MK, Zaucha M, Witter K, Lehmann L, et al. Dynamic changes in circulating T follicular helper cell composition predict neutralising antibody responses after yellow fever vaccination. *Clin Transl Immunol*. (2020) 9:e1129. doi: 10.1002/cti.1129
58. Yasutomi M, Christiaansen AF, Imai N, Martin-Orozco N, Forst CV, Chen G, et al. CD226 and TIGIT cooperate in the differentiation and maturation of human Tfh cells. *Front Immunol*. (2022) 13. doi: 10.3389/fimmu.2022.840457
59. Elgueta R, Benson MJ, De Vries VC, Wasiuk A, Guo Y, Noelle RJ. Molecular mechanism and function of CD40/CD40L engagement in the immune system. *Immunol Rev*. (2009) 229:152–72. doi: 10.1111/j.1600-065X.2009.00782.x
60. Weinstein JS, Herman EI, Lainez B, Licona-Limón P, Esplugues E, Flavell R, et al. TFH cells progressively differentiate to regulate the germinal center response. *Nat Immunol*. (2016) 17:1197–205. doi: 10.1038/ni.3554
61. Gonzalez DG, Cote CM, Patel JR, Smith CB, Zhang Y, Nickerson KM, et al. Nonredundant roles of IL-21 and IL-4 in the phased initiation of germinal center B cells and subsequent self-renewal transitions. *J Immunol*. (2018) 201:3569–79. doi: 10.4049/jimmunol.1500497
62. Hsu HC, Yang PA, Wang J, Wu Q, Myers R, Chen J, et al. Interleukin 17-producing T helper cells and interleukin 17 orchestrate autoreactive germinal center development in autoimmune BXD2 mice. *Nat Immunol*. (2008) 9:166–75. doi: 10.1038/ni1552
63. Mitsdoerffer M, Lee Y, Jäger A, Kim HJ, Korn T, Kolls JK, et al. Proinflammatory T helper type 17 cells are effective B-cell helpers. *Proc Natl Acad Sci U.S.A.* (2010) 107:14292–7. doi: 10.1073/pnas.1009234107
64. Ding Y, Li J, Wu Q, Yang P, Luo B, Xie S, et al. IL-17RA is essential for optimal localization of follicular Th cells in the germinal center light zone to promote autoantibody-producing B cells. *J Immunol*. (2013) 191:1614–24. doi: 10.4049/jimmunol.1300479
65. Jackson SW, Jacobs HM, Arkatkar T, Dam EM, Scharping NE, Kolhatkar NS, et al. B cell IFN- $\gamma$  receptor signaling promotes autoimmune germinal centers via cell-intrinsic induction of BCL-6. *J Exp Med*. (2016) 213:733–50. doi: 10.1084/jem.20151724
66. Domeier PP, Chodisetti SB, Soni C, Schell SL, Elias MJ, Wong EB, et al. IFN- $\gamma$  receptor and STAT1 signaling in B cells are central to spontaneous germinal center formation and autoimmunity. *J Exp Med*. (2016) 213:715–32. doi: 10.1084/jem.20151722
67. Ryg-Cornejo V, Ioannidis LJ, Ly A, Chiu CY, Tellier J, Hill DL, et al. Severe malaria infections impair germinal center responses by inhibiting T follicular helper cell differentiation. *Cell Rep*. (2016) 14:68–81. doi: 10.1016/j.celrep.2015.12.006
68. Obeng-Adjei N, Portugal S, Holla P, Li S, Sohn H, Ambegaonkar A, et al. Malaria-induced interferon- $\gamma$  drives the expansion of Tbet<sup>hi</sup> atypical memory B cells. *PLoS Pathog*. (2017) 13:e1006576. doi: 10.1371/journal.ppat.1006576
69. Arroyo-Diaz NM, Bachus H, Papillion A, Randall TD, Akther J, Rosenberg AF, et al. Interferon- $\gamma$  production by Tfh cells is required for CXCR3+ pre-memory B cell differentiation and subsequent lung-resident memory B cell responses. *Immunity*. (2023) 56:2358–2372.e5. doi: 10.1016/j.immuni.2023.08.015
70. He R, Zheng X, Zhang J, Liu B, Wang Q, Wu Q, et al. SARS-CoV-2 spike-specific TFH cells exhibit unique responses in infected and vaccinated individuals. *Signal Transduct Target Ther*. (2023) 8:393. doi: 10.1038/s41392-023-01650-x
71. Woodruff MC, Ramonell RP, Nguyen DC, Cashman KS, Saini AS, Haddad NS, et al. Extrafollicular B cell responses correlate with neutralizing antibodies and morbidity in COVID-19. *Nat Immunol*. (2020) 21:1506–16. doi: 10.1038/s41590-020-00814-z
72. Witkowski M, Tizian C, Ferreira-Gomes M, Niemeyer D, Jones TC, Heinrich F, et al. Untimely TGF $\beta$  responses in COVID-19 limit antiviral functions of NK cells. *Nature*. (2021) 600:295–301. doi: 10.1038/s41586-021-04142-6
73. Hill DL, Pierson W, Bolland DJ, Mkindi C, Carr EJ, Wang J, et al. The adjuvant GLA-SE promotes human Tfh cell expansion and emergence of public TCR $\beta$  clonotypes. *J Exp Med*. (2019) 216:1857–73. doi: 10.1084/jem.20190301